Article:
Di Natali, C, Beccani, M, Obstein, KL et al. (2014) A wireless platform for in vivo measurement of resistance properties of the gastrointestinal tract. Physiological Measurement, 35 (7). pp. 1197-1214. ISSN: 0967-3334

https://doi.org/10.1088/0967-3334/35/7/1197

A Wireless Platform for *In Vivo* Measurement of Resistance Properties of the Gastrointestinal Tract

C Di Natali[1], M Beccani[1], K L Obstein[2,1] and P Valdastri[1,2].

[1] STORM Lab, Department of Mechanical Engineering, Vanderbilt University, Nashville, TN 37235-1592, USA

[2] Division of Gastroenterology, Hepatology, and Nutrition, Vanderbilt University Medical Center, Nashville, TN 37235-1592, USA

E-mail: p.valdastri@vanderbilt.edu

Abstract. Active locomotion of wireless capsule endoscopes has the potential improve the diagnostic yield of this painless technique for the diagnosis of gastrointestinal tract disease. In order to design effective locomotion mechanisms, a quantitative measure of the propelling force required to effectively move a capsule inside the gastrointestinal tract is necessary.

In this study, we introduce a novel wireless platform that is able to measure the force opposing capsule motion, without perturbing the physiologic conditions with physical connections to the outside of the gastrointestinal tract. The platform takes advantage of a wireless capsule that is magnetically coupled with an external permanent magnet. A secondary contribution of this manuscript is to present a real-time method to estimate the axial magnetic force acting on a wireless capsule manipulated by an external magnetic field. In addition to the intermagnetic force, the platform provides real-time measurements of the capsule position, velocity, and acceleration.

The platform was assessed with benchtop trials within a workspace that extends 15 cm from each side of the external permanent magnet, showing average error in estimating the force and the position of less than 0.1 N and 10 mm, respectively. The platform was also able to estimate the dynamic behavior of a known resistant force with an error of 5.45%. Finally, an *in vivo* experiment on a porcine colon model validated the feasibility of measuring the resistant force in opposition to magnetic propulsion of a wireless capsule.

Keywords: Resistant force, intermagnetic force, magnetic force measurement, wireless capsule endoscopy, gastrointestinal endoscopy, colonoscopy, physiology.

PACS numbers: 87.19.R-, 87.19.ru, 87.85.St, 87.85.G-, 87.85.gj, 85.70.Ay, 85.70.Rp

Submitted to: *Physiol. Meas.*

1. Introduction

The gastrointestinal (GI) tract is home to many deadly human diseases. Colorectal cancer (CRC) alone is the third most common cancer in men and the second in women worldwide (*Globocan* 2008). However, most GI diseases can be prevented – or timely cured – if the diagnosis occurs at an early stage of development. For this reason, GI screening is playing an increasingly important role in healthcare systems worldwide (*Centers for Disease Control and Prevention* 2013, Pox et al. 2007).

One method for GI screening that has quickly risen to become the preferred option is flexible endoscopy due to its ability to serve as both a diagnostic and therapeutic modality. Unfortunately, its application is sometimes limited due to its invasiveness, patient intolerance, and the need for sedation. These disadvantages are severe enough for some patients, that millions forgo or avoid recommended screening (*Centers for Disease Control and Prevention* 2013).

Over the past decade, wireless capsule endoscopy (WCE) established itself as a patient-friendly procedure for diagnosis of diseases in the small intestine (Toennies et al. 2010). Specific wireless capsule endoscopes have been proposed for colon inspection, but have not reached the diagnostic accuracy of standard colonoscopy (Eliakim et al. 2009, Spada et al. 2012). One of the main limitations of commercially available capsule endoscopes is passive locomotion (Valdastri, Simi & Webster III 2012). It is desirable for the endoscopist to be able to maneuver the camera arbitrarily rather than relying on peristalsis to drive the capsule for adequate visualization of GI mucosa. For this reason, a relevant number of technical solutions have been recently proposed to provide active locomotion to WCE, including walking (Valdastri et al. 2009) or crawling (Sliker et al. 2012) capsules, remote magnetic manipulation (Ciuti et al. 2010, Mahoney & Abbott 2012, Rey et al. 2012, Keller et al. 2011), and hybrid approaches (Simi et al. 2010, Yim & Sitti 2012).

As mentioned in (Terry et al. 2012), the engineers designing active locomotion mechanisms for WCE would greatly benefit from having a quantitative measure of the propelling forces required to effectively move a capsule in the targeted GI segment. Several works have been published recently that address this scientific need. The proposed methods to measure resistant properties of the GI tract range from *ex vivo* trials performed with benchtop equipment (Wang & Meng 2010, Kim et al. 2006, Lyle et al. 2013, Zhou et al. 2013), to dedicated instrumentation that can acquire data *in vivo* during a surgical procedure (Samsom et al. 1998, Terry et al. 2012); however, the main limitation to all of the proposed methods thus far has been that a wired connection is always used to perform the measurement. In (Wang & Meng 2010), a capsule mock-up sliding inside an intestinal lumen is pulled by a load cell through a string, whereas a multi-lumen connection is used in (Terry et al. 2012) to operate the measurement device deployed in the small intestine of a living pig. Having a physical connection to the outside of the GI tract throughout the measurement has the potential to affect the readings and compromise the results integrity. Measuring the resistance properties of the

GI tract with a wireless device would allow for preservation of physiological conditions – including the contribution of surrounding organs – and to obtain measurements that are closer to the actual forces that an active capsule endoscope must face in navigating the GI tract.

The main contribution of this paper is to present – for the first time – a wireless platform for the measurement of the resistant force that an active capsule must overcome in order to move inside the GI tract. The proposed platform is validated with benchtop trials and through an *in vivo* experiment using a porcine colon model. A secondary contribution of this paper is to present a real-time method to estimate the axial magnetic force acting on a wireless capsule manipulated by an external magnetic field. An extensive quantification of resistance properties of the different GI segments – outside the scope of this paper – can then be obtained by adopting the proposed methods. The same approach would also enable gathering reliable data for implementing realistic biomechanical models of the GI tract (Kim et al. 2007, Bellini et al. 2011, Zhang et al. 2012, Zhou et al. 2013).

2. Materials and Methods

2.1. Method Overview

A common method to measure the resistance properties of the intestine is to impose a motion to a capsule mock-up inside the lumen and to measure the associated force profile (Wang & Meng 2010, Zhang et al. 2012, Zhou et al. 2013). An equivalent approach, schematically represented in Fig. 1, consists of imposing an increasing force $\mathbf{F}_a$ to the capsule and recording the motion profile to understand when the applied force $\mathbf{F}_a$ overcomes the resistant force $\mathbf{F}_r$. Referring to the instant when motion starts as t_0 and assuming a static equilibrium until that moment, the value $\mathbf{F}_a(t_0)$=$\mathbf{F}_r(t_0)$ quantifies the static resistant force that an active capsule must overcome to begin its motion. Then, as the motion builds up, driven by $\mathbf{F}_a$ increases, the system moves away from the equilibrium and the following equation can be used to describe its dynamics:

$$\mathbf{F}_{tot} = \mathbf{F}_a - \mathbf{F}_r = m\ddot{\mathbf{d}}, \tag{1}$$

where $\mathbf{d}$ is the position of the capsule center of mass O_c, while m is the capsule mass.

The platform described in this paper allows application of a force $\mathbf{F}_a$ to a capsule without the need for a tethered connection – thus preserving physiologic condition during *in vivo* measurements. This is achieved by leveraging magnetic coupling between an external permanent magnet (EPM) and a magnet embedded inside the capsule. The applied force $\mathbf{F}_a$, the position $\mathbf{d}$, and the acceleration $\ddot{\mathbf{d}}$ are measured wirelessly in real time with respect to a reference frame $\{\mathbf{x}_m, \mathbf{y}_m, \mathbf{z}_m\}$ on the EPM. While just $\mathbf{F}_a$ and $\ddot{\mathbf{d}}$ would be sufficient for a complete characterization of $\mathbf{F}_r$, real-time knowledge of $\mathbf{d}$ allows adjustment of the setup during *in vivo* trials and to record the distance traveled by the capsule for each measurement. In addition, the capsule velocity $\dot{\mathbf{d}}$ can be calculated as the first derivative of $\mathbf{d}$ to provide additional information about the motion profile. The

methods for measuring all of the quantities mentioned will be described in the following sections of the paper.

The applied force $\mathbf{F}_a$ can be adjusted by controlling the position of the EPM. This can be achieved by a robotic manipulator, as proposed for benchtop validation in sections 3.1 and 3.2. Alternatively, the EPM position can be manually adjusted by an operator until the capsule starts its motion, as indicated by the real-time measurement of $\dot{\mathbf{d}}$ and $\ddot{\mathbf{d}}$. This approach was used for the *in vivo* validation of the platform, as further detailed in section 3.3.

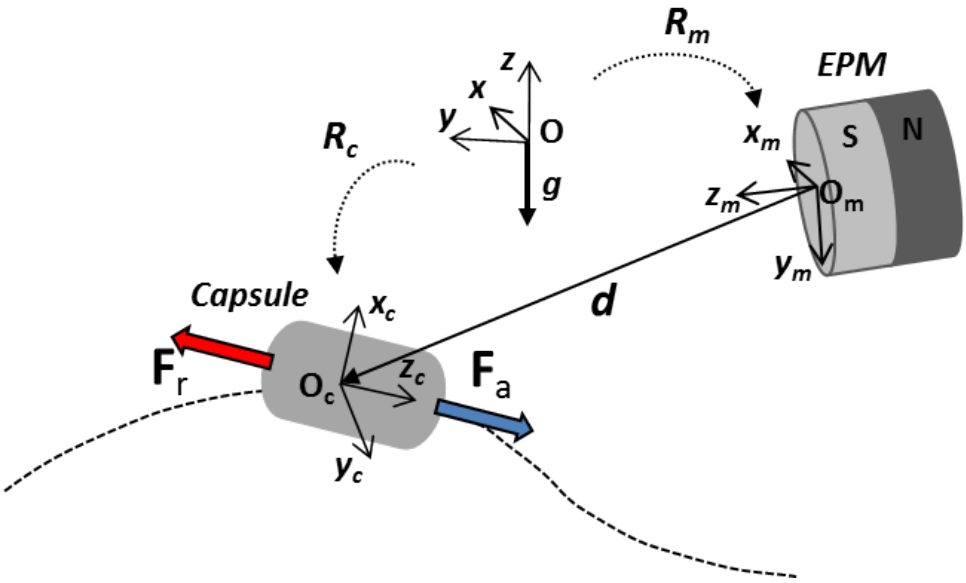

Figure 1. Schematic representation of the principle of operation. The attraction force $\mathbf{F}_a$ is generated by magnetic coupling between an external permanent magnet (EPM) and a magnet embedded in the capsule. The intermagnetic force $\mathbf{F}_a$ and the capsule position $\mathbf{d}$ with respect to the EPM are recorded wirelessly in real time. $\mathbf{F}_r$ is the resistant force, $\mathbf{g}$ is the gravitational acceleration vector, R_c is the rotational matrix of the capsule reference frame with respect to the global Cartesian coordinate system, while R_m is the rotational matrix of the reference frame at the EPM with respect to the global Cartesian coordinate system.

2.2. Platform Overview

The platform is composed of a wireless capsule, the EPM, and a personal computer (PC) connected to a wireless transceiver via the universal serial bus (USB) port. The real-time algorithm runs on the PC and communicates with the capsule through the USB transceiver. The EPM is a NdFeB (magnetization N52, magnetic remanence 1.48 T) cylindrical permanent magnet with axial magnetization, as represented in Fig. 1. The EPM diameter and length are both equal to 50 mm, while the mass is 772 g. A triaxial accelerometer (LIS331DL, STMicroelectronics, Switzerland) – used as inclinometer – is mounted on the EPM to provide pitch and yaw angles of $\{\mathbf{x}_m, \mathbf{y}_m, \mathbf{z}_m\}$ with respect

to the global frame $\{\mathbf{x}, \mathbf{y}, \mathbf{z}\}$. These angles are used for the localization algorithm – as described in section 2.3.2 – and fed directly to the PC through a 16-bit acquisition board (DAQ USB-6211, National Instruments, USA).

The wireless capsule, schematically represented in Fig. 2, hosts a force and motion sensing module (FMSM), wireless communication, and power supply. Each of these modules are described in detail in the following subsections. The outer shell was fabricated in biocompatible material – polyether-ether-ketone, PEEK – by traditional machining. The current prototype is 60 mm in length, 18 mm in diameter, 21 g in mass. For comparison, the Given Imaging PillCam SB2 is 26 mm in length, 11 mm in diameter, 3.5 g in mass. Having a larger capsule for measuring resistance properties does not jeopardize the relevance of the results, as long as the animal model selected takes into account the appropriate scaling factors (i.e., diameter and size of human colon (Hounnou et al. 2002), diameter and size of porcine colon as a function of body weight (Miller & Ullrey 1987), resistant properties of capsule endoscopes as a function of size, surface and diameter of the capsule (Kim et al. 2007, Wang & Meng 2010)).

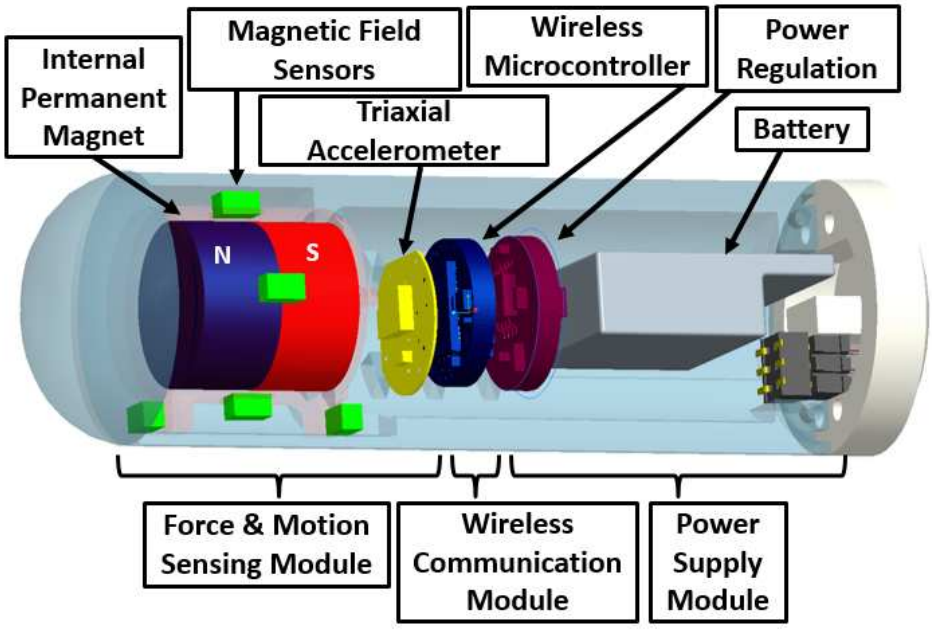

Figure 2. Schematic view of the wireless capsule for measuring resistant properties of the GI tract.

2.3. Force and Motion Sensing Module

The FMSM hosts the internal permanent magnet (IPM) that couples with the EPM to generate the force $\mathbf{F}_a$ applied to the wireless capsule. The selected IPM is an off-the-shelf NdFeB (N52) cylindrical magnet axially magnetized with 1.48 T of magnetic remanence, 11 mm in diameter and 11 mm in height. This EPM-IPM couple generates an intermagnetic force of 1 N when the two magnets are separated by 8 cm and the axes

$\mathbf{z}_c$ and $\mathbf{z}_m$ are aligned.

The FMSM is responsible for acquiring the real time sensor readings required to estimate $\mathbf{F}_a$, $\mathbf{d}$, and $\ddot{\mathbf{d}}$. The transducers embedded in the module are six linear magnetic field sensors (MFS) based on the Hall effect (A1391, Allegro Microsystems, USA) and a 16-bit digital triaxial accelerometer with serial peripheral interface (SPI) (LIS331DL, STMicroelectronics, Switzerland, sensitivity of 176.6 mm/s^2). As represented in Fig. 3, the MFS are mounted two by two orthogonally around the IPM. Each MFS measures the component of the magnetic field $\mathbf{B}$ that is perpendicular to the IPM surface at the MFS location (i.e., referring to Fig. 3, MFS_i measures the component B_i for i ranging from 1 to 6). Similarly to (Miller et al. 2012), the position of each MFS has been selected to minimize the constant bias in the reading due to the field generated by the IPM. This explains why the two MFS along the z_c direction (MFS_5 and MFS_6) are placed at the edge of the IPM, rather than on its main axis. The bias from the IPM that still remains in each MFS output is treated as an offset and filtered out from the measurements. The MFS analog outputs are acquired by the 12-bit analog to digital converter (ADC) of the wireless microcontroller (CC2530, Texas Instruments, USA) integrated in the communication module. The digitized magnetic field signal results in a sensitivity of 64 μT.

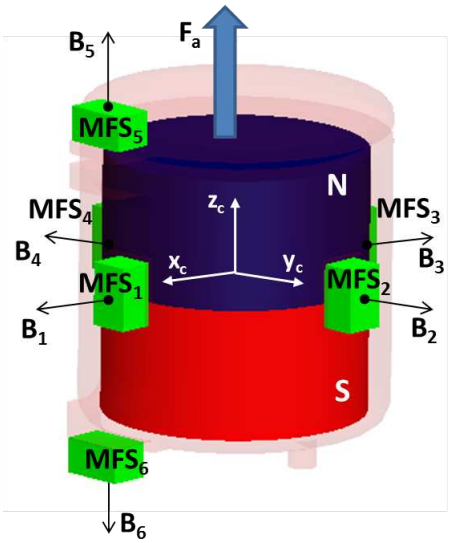

Figure 3. Magnetic field sensor (MFS) position with respect to the internal permanent magnet.

2.3.1. Intermagnetic Force Estimation The goal of this section is to describe a new method to estimate the intermagnetic force $\mathbf{F}_a$ acting on the main axis of the IPM (i.e., $\mathbf{z}_c$ in Fig. 3) under the effect of an external magnetic field $\mathbf{B}_{ext}$. Current approaches either rely on the dipole-dipole magnetic field approximation (Petruska & Abbott 2013) or finite element integration (Salerno et al. 2013). The first method provides an analytical expression of the magnetic field that is accurate at a certain distance from the magnetic

field source. On the other hand, finite element integration allows the procurement of accurate results at the price of long computational times (Salerno et al. 2013).

The method proposed in this study is based on the finite element integration of real-time sensor data. The analytical formulation derived in this subsection, can be used to estimate $\mathbf{F}_a$ in real time as a direct function of four MFS readings (i.e., MFS_1 to MFS_4) with low computational costs.

As described in (Furlani 2001), the magnetic force $\mathbf{F}$ acting on a permanent magnet under the effect of an external magnetic field $\mathbf{B}_{ext}$ can be expressed by applying the equivalent current magnetic model:

$$\mathbf{F} = \oint_S \mathbf{j}_m \times \mathbf{B}_{ext} \delta S, \tag{2}$$

where S is the IPM surface and $\mathbf{j}_m$ is the equivalent current surface density on the IPM. The current density $\mathbf{j}_m$ is derived from:

$$\mathbf{j}_m = \mathbf{M}_{IPM} \times \mathbf{n}, \tag{3}$$

where $\mathbf{M}_{IPM}$ is the IPM magnetization vector, having expression $B_r/\mu_0 \hat{\mathbf{z}}$ – with $\hat{\mathbf{z}}$ denoting the unit vector along $\mathbf{z}_c$, while $\mathbf{n}$ is the normal vector coming out from the IPM surface, as represented in Fig. 4.A.

From Eq. 3, it is possible to conclude that – given an axially magnetized cylindrical IPM, $\mathbf{j}_m$ only flows on the lateral surface. Therefore, the component of $\mathbf{B}_{ext}$ along $\hat{\mathbf{z}}$ does not contribute to the estimation of $\mathbf{F}$ through the equivalent current magnetic model (Eq. 2).

In order to provide an analytical expression for Eq. 2, it is possible to take advantage of the axial symmetry of our problem, thus dividing the cross-section of the IPM into four identical quadrants, as represented in Fig. 4.A. Focusing on the u-th quadrant and defining θ as the angular coordinate (see Fig. 4.B), it is possible to express the current density $\mathbf{j}_m$ as:

$$\mathbf{j}_m(\theta) = M_{IPM}[-sin(\theta)\hat{\mathbf{x}} + cos(\theta)\hat{\mathbf{y}}], \tag{4}$$

where $\hat{\mathbf{x}}$ and $\hat{\mathbf{y}}$ are the unit vectors along $\mathbf{x}_c$ and $\mathbf{y}_c$, respectively.

In the proposed capsule design, the magnetic field $\mathbf{B}_u$ is measured by the MFS_u placed at $\theta = \pi/4$ in each quadrant and can be expressed as:

$$\mathbf{B}_u = B_u[cos(u\frac{\pi}{2} - \frac{\pi}{4})\hat{\mathbf{x}} + sin(u\frac{\pi}{2} - \frac{\pi}{4})\hat{\mathbf{y}}], \tag{5}$$

where B_u is the numerical value recorded by MFS_u and u ranges from 1 to 4.

Assuming that the magnetic field in each quadrant is coincident with the magnetic field $\mathbf{B}_u$, the surface integral in Eq. 2 can be simplified in the following sum:

$$\mathbf{F} = \sum_{u=1}^{4} \sum_{\theta=0}^{\pi/2} (\mathbf{j}_m \times \mathbf{B}_u) \Delta S = \sum_{u=1}^{4} sgn[cos(u\frac{\pi}{2} - \frac{\pi}{4})] \sum_{\theta=0}^{\pi/2} f_u \Delta S \hat{\mathbf{z}}, \tag{6}$$

where *sgn* is the sign function, ΔS is the lateral surface of one quadrant of the IPM and is equal to $\pi/2rh$, in which r is the radius and h the height of IPM. f_u is the contribution

to the module of the intermagnetic force acting on the u-th quadrant at a given θ and can be expressed as:

$$f_u = M_{IPM}\frac{B_u}{\sqrt{2}}(sin(\theta) + cos(\theta)). \tag{7}$$

Considering that

$$\sum_{\theta=0}^{\pi/2}[sin(\theta) + cos(\theta)] = \Theta = 1.27, \tag{8}$$

the analytical expression for the intermagnetic force becomes:

$$\mathbf{F} = \sum_{u=1}^{4} sgn[cos(u\frac{\pi}{2} - \frac{\pi}{4})]\frac{\Theta}{\sqrt{2}}M_{IPM}\frac{\pi}{2}rhB_u\hat{\mathbf{z}} \tag{9}$$

This simple equation can be used to get a fast estimate of the intermagnetic force $\mathbf{F}_a$ from the readings of MFS_1, MFS_2, MFS_3, MFS_4. Considering the computational platform described in section 2.5, the time required to estimate the magnetic force is 0.18 ± 0.05 ms.

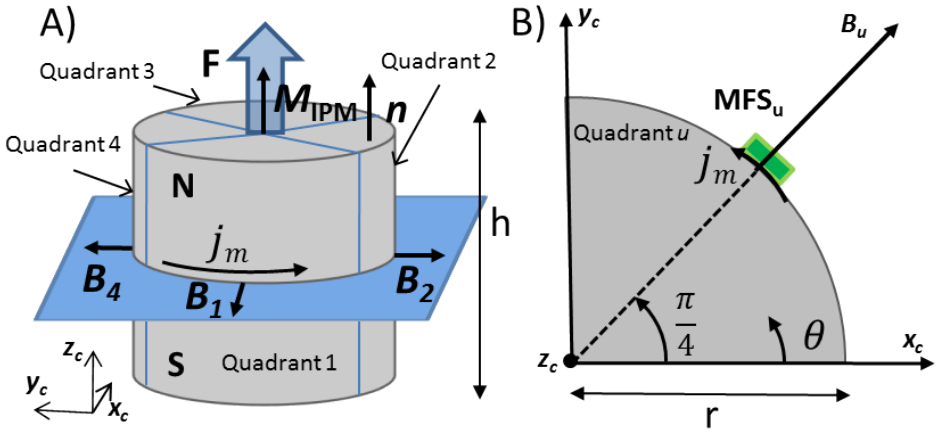

Figure 4. (A) Lateral view of the IPM. (B) Schematic view of the i-th quadrant of the IPM.

2.3.2. Capsule Motion Estimation The information related to capsule motion that the proposed platform provides in real time are: (1) capsule acceleration $\ddot{\mathbf{d}}$, (2) indication that motion has started, and (3) capsule position $\mathbf{d}$ with respect to the EPM.

The capsule acceleration $\ddot{\mathbf{d}}$ is directly measured by the onboard triaxial accelerometer. The same sensor is also used to detect the instant when capsule motion begins. In particular, it is possible to assume that the capsule begins moving whenever the following equation is satisfied:

$$\|\ddot{\mathbf{d}} - \mathbf{g}\| \geq T, \tag{10}$$

where $\mathbf{g}$ is the gravitational acceleration vector and T is a threshold set to 5% of $|\mathbf{g}|$ (i.e., 0.49 m/s^2). The threshold T was defined by experimental calibration to prevent

false positives due to noise of the measurement or movements that were not related to capsule motion. Another method to confirm that the capsule is moving – probably better suited for *a posteriori* data interpretation – consists of analyzing the position $\mathbf{d}$ and the velocity $\dot{\mathbf{d}}$ profiles, both acquired by the proposed platform. This approach would allow for detection of motion profiles that begin without a sudden change in acceleration.

The methods and the algorithm used to solve the electromagnetic inverse problem (i.e., to estimate the capsule position $\mathbf{d}$ with respect to the EPM) by leveraging onboard sensor readings are reported in (Di Natali et al. 2013, Beccani et al. 2013). Briefly, using an average of the measurements provide by MFSs lying on the same axis, the three components of the magnetic field vector $\mathbf{B}_{ext}$ are measured at the capsule center. The $\mathbf{B}_{ext}$ vector is then rotated according to

$$\mathbf{B}'_{ext} = R_m^T R_c R_m \mathbf{B}_{ext}, \tag{11}$$

where R_c is the rotational matrix of the capsule reference frame with respect to the global Cartesian coordinate system, while R_m is the rotational matrix of the reference frame at the EPM with respect to the global Cartesian coordinate system, as represented in Fig. 1. The matrix R_c is obtained in real time from the readings acquired by the inclinometer integrated in the capsule, while R_m is derived from the data acquired by the inclinometer mounted on the EPM.

Then, a search within a precalculated magnetic field map is performed to find the capsule position $\mathbf{d}$ that would match with the actual magnetic field vector $\mathbf{B}'_{ext}$. The magnetic map – associating each point $\mathbf{d}$ within the workspace to the related magnetic field intensity $\mathbf{B}'_{ext}$ – denotes the search space for the inverse localization procedure. The effective localization workspace – defined as the search space of potential capsule positions – extends 15 cm away from each side of the EPM. The only limitation of this localization method is that capsule or EPM orientation around the $\mathbf{z}$ axis of the global Cartesian coordinate system cannot be measured by the inclinometers used to generate R_c and R_m. This sets a constraint on the experimental procedure that the capsule and the EPM must lay on parallel vertical planes for the entire duration of the measurement. If taken into account when designing the measurement protocol, this constraint does not limit the effectiveness of the platform in acquiring reliable *in vivo* data on intestinal resistance properties, as demonstrated in section 3.3.

The capsule velocity and acceleration can be estimated as the first and second time derivative of $\mathbf{d}$, respectively. However, direct measurement of $\ddot{\mathbf{d}}$ from the accelerometer provides better accuracy, as briefly discussed in section 3.1. Considering the computational platform described in section 2.5, the time required to estimate the capsule position with respect the magnetic source is 16 ± 2.5 ms.

2.4. Communication and Power Supply Modules

The readings of the sensors integrated in the FMSM are acquired by the onboard wireless microcontroller. An acquisition cycle starts from sampling seven analog inputs – six

connected to the MFS outputs, and one to the battery for monitoring the charge status. Then, the three digitized values of acceleration are received from the 128 kbyte/s SPI bus connected to the onboard accelerometer. This dataset is acquired every 4.4 ms by the microcontroller and used to build a 32-byte package together with the wireless signal strength indicator, the battery level, an incremental package number identifier, and the start/stop bytes. This package is then transmitted by the wireless microcontroller to the external transceiver over a 2.4 GHz carrier frequency, with a refresh time of 6 ms (wireless data throughput 42.4 kbit/s), resulting in sampling rate of 166 Hz. The external transceiver is based on an identical microcontroller (CC2530, Texas Instruments, USA) which communicates with the PC through a USB-serial converter (UM232R, FTDI, UK).

The power supply module embeds a low-dropout voltage regulator (LDO) (TPS73xx, Texas Instruments, USA) to provide a stable supply to both FPMS and communication modules. In order to limit the current consumption when the device is not acquiring measurements, a digital output of the microcontroller can drive the SLEEP pin of all the MFS. This results in a current consumption which varies between 400 μA, when the microcontroller is in low power mode, and 20 mA when it is in IDLE mode with the radio active. Average current consumption rises to 48 mA during a single cycle of sensor data acquisition and wireless transmission. The power source used is a 50 mAh, 3.7 V rechargeable LiPo battery (Shenzhen Hondark Electronics Co., Ltd., China, 12 mm $\times$ 15 mm $\times$ 3 mm in size).

2.5. User Interface

A multi-thread C++ WIN32 application running on the PC unbundles the data and shares them via TCP-IP communication with a second application (developed in MATLAB, Mathworks, USA), which runs in parallel to implement the estimation algorithms and the user interface. The data transfer rate between the two applications is 30 Hz, while the refresh time for capsule position $\mathbf{d}$, acceleration $\ddot{\mathbf{d}}$, and intermagnetic force $\mathbf{F}_a$ is 50 ms (refresh rate 20 Hz). Two real-time plots are displayed on the main screen, as represented on the right side of Fig. 5. The applied intermagnetic force $\mathbf{F}_a$ is shown on the left as a function of time, while the position and orientation of the capsule reference frame $\{\mathbf{x}_c, \mathbf{y}_c, \mathbf{z}_c\}$ with respect to the EPM reference frame $\{\mathbf{x}_m, \mathbf{y}_m, \mathbf{z}_m\}$ are displayed in real time on the right side. Numerical values for capsule position $\mathbf{d}$ and velocity $\dot{\mathbf{d}}$ are also shown, together with the most current values of the battery voltage and the wireless signal strength indicator. Capsule velocity $\dot{\mathbf{d}}$ is filtered by applying a 5-element moving average. A visual indicator alerts the user every time that motion starts, in agreement with Eq. 10. The user interface also allows the user to set the initial bias for the measurement and to record the data in a spreadsheet file.

3. Platform Assessment

3.1. Validation of Intermagnetic Force and Capsule Position Estimation

The setup used to assess the intermagnetic force and capsule position estimation is represented in Fig. 5. The wireless capsule was mounted on a rigid support connected to a six-axis load cell (NANO17, ATI Industrial Automation, USA, resolution 1/160 N). The load cell output was assumed as reference for $\mathbf{F}_a$ measurement. The EPM was mounted at the end effector of a six-degree of freedom robotic manipulator (RV6SDL, Mitsubishi Corp., Japan). The robotic arm allowed the EPM to move inside the workspace instead of the capsule, providing a reference for the EPM-capsule separation vector $\mathbf{d}$ via the built-in encoders (resolution of 1 μm). A second six-axis load cell (MINI 45, ATI Industrial Automation, USA, resolution 1/16 N) was placed in between the EPM and the robotic arm. This load cell was used as shared control input (Ciuti et al. 2012) to impose the desired EPM trajectories during the validation. The capsule and the EPM reference frame orientations are shown in Fig. 5, together with the position of the external inclinometer.

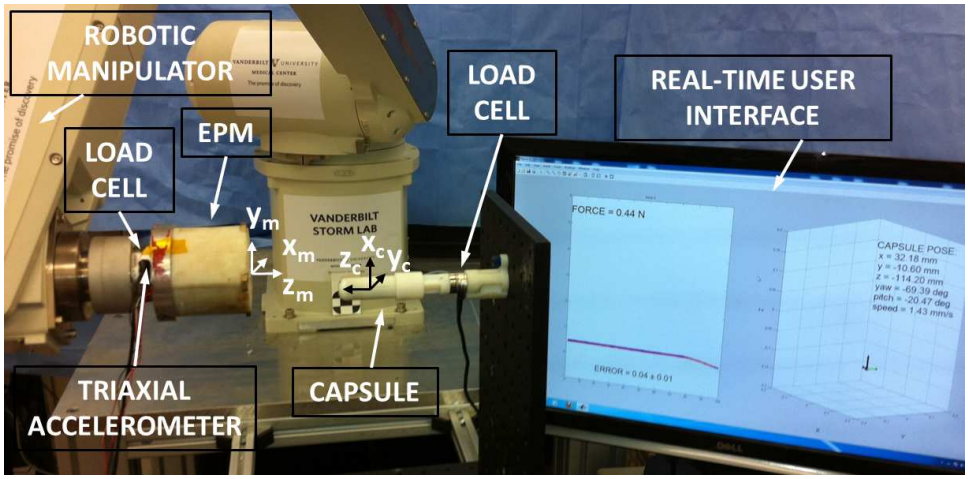

Figure 5. Experimental setup used to assess the intermagnetic force and capsule position estimation.

A total of 20 trials were performed by moving the EPM inside a workspace defined as $\{x_c \in [0cm..15cm], y_c \in [-15cm..15cm], z_c \in [0cm..15cm]\}$. The space with $\mathbf{x}_c$ negative was not considered, since it is not accessible for the EPM during *in vivo* trials. For each measurement, the EPM was moved along the $\mathbf{z}_c$ axis from 15 cm to 5 cm away from the capsule and back. The EPM position along the $\mathbf{x}_c$ and $\mathbf{y}_c$ axes was varied randomly by the operator for each trial. Rotations of the EPM around $\mathbf{y}_m$ were avoided to satisfy the constraint mentioned in section 2.3.2. The estimated modules of $\mathbf{F}_a$ and $\mathbf{d}$ are plotted in Fig. 6 together with the module of the EPM position, as derived from the manipulator encoders, and the module of the force along $\mathbf{z}_c$, as measured by the load cell connected to the capsule. These plots are related to a part of a trial where the EPM was moved mainly along the $\mathbf{z}_c$ axis for about 9 cm.

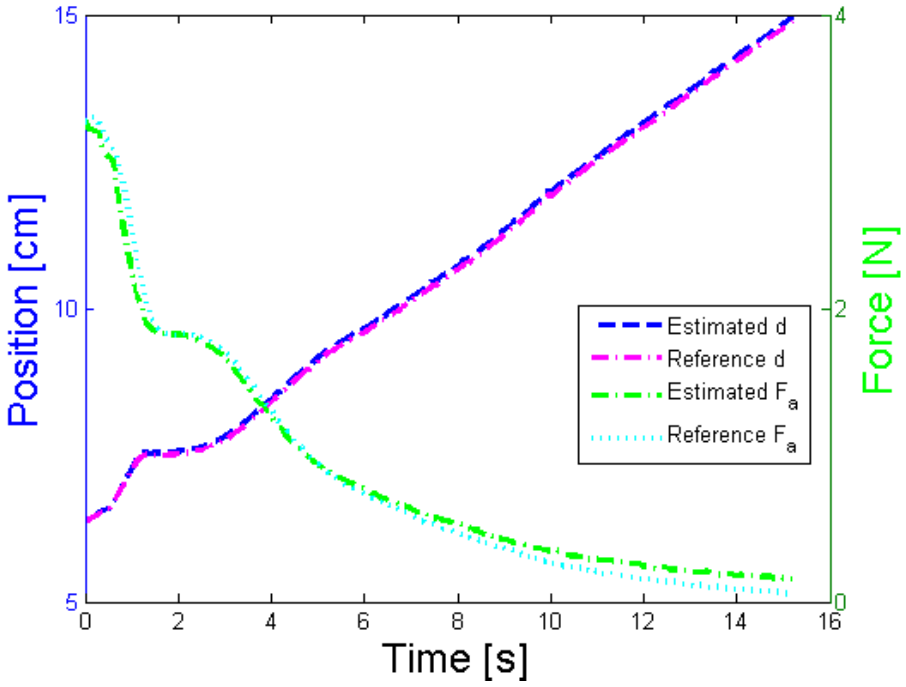

Figure 6. Modules of the estimated force $\mathbf{F}_a$, the reference force along $\mathbf{z}_c$, the estimated position $\mathbf{d}$, and the reference position as measured by the robotic manipulator encoders for part of a trial where the EPM was moved mainly along the $\mathbf{z}_c$ axis (i.e., from {x_c=8 mm, y_c=-10 mm, z_c=62 mm} to {x_c=8 mm, y_c=-5 mm, z_c=148 mm}.

The data recorded during the 20 trials were statistically analyzed to derive the average error and the standard deviation of both $\mathbf{F}_a$ and $\mathbf{d}$ within the entire workspace. The proposed method presented an average error of 0.079 ± 0.049 N in estimating the intermagnetic force $\mathbf{F}_a$. As regard to capsule position $\mathbf{d}$, the average estimation error was 3.34 ± 2.23 mm for the x component, 4.12 ± 2.88 mm for the y component, and 6.45 ± 4.84 mm for z component. Given these results, it is possible to estimate how the uncertainty in position would propagate to the acceleration if this is calculated as the second time derivative of $\mathbf{d}$. By applying the Kline-McClintock method (Kline & McClintock 1953), the uncertainty of $\ddot{\mathbf{d}}$ as a derived measurement from $\mathbf{d}$ would be in the order of 0.6 m/s^2, thus demonstrating that the $\ddot{\mathbf{d}}$ is more reliably quantified by the onboard accelerometer.

3.2. Validation of Resistant Force Estimation

The goal of this experiment was to assess the entire platform in reconstructing a known resistant force applied to the capsule. As represented in Fig. 7, the capsule was connected to a support frame through a two-element metallic spring (180-A W.B., Jones Spring CO, Inc.) with a nominal elastic constant k of 192.6 N/m. The EPM – mounted on the robotic manipulator – was approached to the capsule from the opposite side

of the spring in steps of 2 mm, until the magnetic force did not overcome the elastic force and the capsule started accelerating towards the EPM. Foam placed on top of the EPM prevented damaging the capsule. Spring elongation Δx was measured by real-time image analysis. This approach allowed an estimation of the capsule motion profile that was independent and one order of magnitude more accurate than the method proposed in section 2.3.2. In particular, an optical tracker was implemented by acquiring and elaborating images from a USB camera (MacAlly MegaCam 2.0 Megapixel, 30 fps with 1600×1200 pixel resolution) to track the position of a marker painted on the capsule. Calibration of the tracker consisted of finding the spatial resolution in terms of mm/pixel and defining the image window where the capsule would move during the experiment. Overall accuracy and sampling rate for Δx as measured by optical tracking was 0.15 mm and 35 ms, respectively.

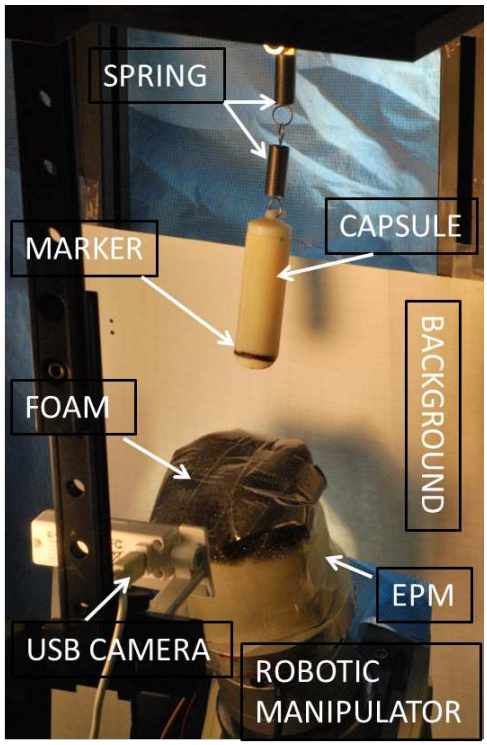

Figure 7. Experimental setup used to validate the reconstruction of a known resistant force.

The plot in Fig. 8.A shows with a blue solid line the module of the estimated resistant force $|\mathbf{F}_r^{est}| = |\mathbf{F}_a - m\ddot{\mathbf{d}}|$, where $\mathbf{F}_a$ is obtained with the method described in section 2.3.1, m is the mass of the capsule, and $\ddot{\mathbf{d}}$ is measured by the onboard accelerometer. On the same plot, the dashed green line represents the reference for the module of the resistant force, obtained by $|\mathbf{F}_r| = k\Delta x$, where k is the nominal constant of the spring and Δx is the spring elongation as measured by the optical tracker. The dashed vertical line indicates the instant when the EPM was moved towards the capsule by 2 mm, but the magnetic force was not enough to overcome the elastic force. The

solid vertical line indicates a second 2-mm motion of the EPM towards the capsule. This event is almost coincident with the start of capsule motion as detected by Eq. 10.

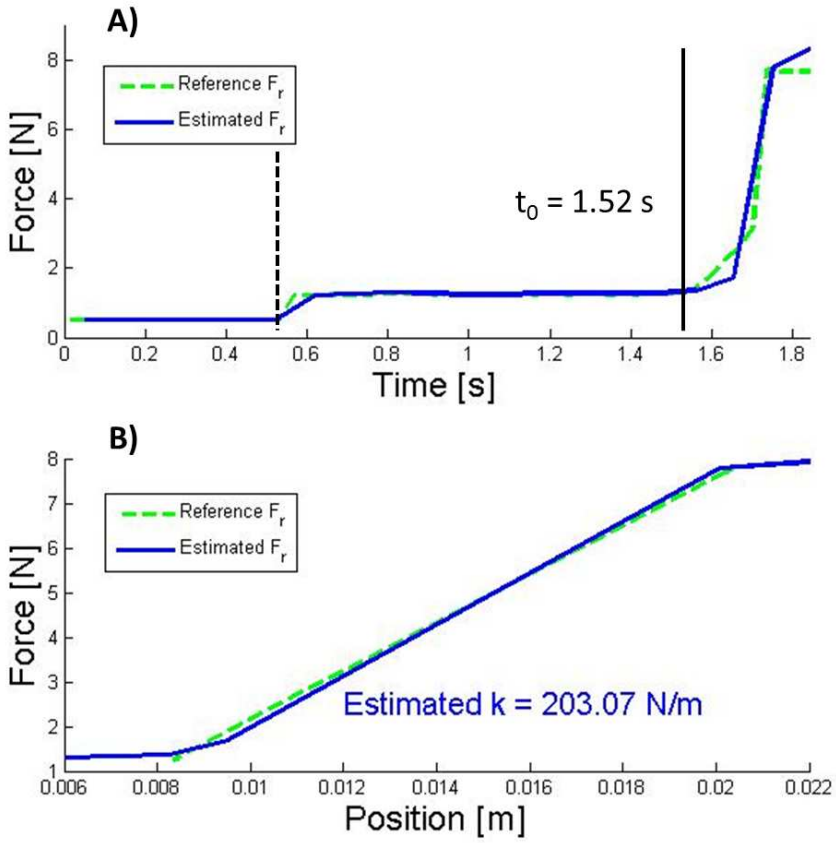

Figure 8. (A) Time variation of the modules of the resistant force estimated with the proposed method (solid blue line) and reference (dashed green line). The dashed vertical line indicates the instant when the EPM was moved towards the capsule by 2 mm, but the the magnetic force was not enough to overcome the elastic force. The solid vertical line indicates a second 2-mm motion of the EPM towards the capsule. This event is almost coincident with the start of capsule motion as detected by Eq. 10. (B) Modules of the resistant force estimated with the proposed method (solid blue line) and reference (dashed green line) plotted as a function of capsule position.

Focusing on the data acquired during the elongation phase of the spring, Fig. 7.B shows $|\mathbf{F}_r^{est}|$ (solid blue line) as a function of the capsule position $|\mathbf{d}|$, as estimated by the method described in section 2.3.2. On the same figure, the reference $|\mathbf{F}_r|$ (dashed green line) is plotted as a function of the capsule position measured by the optical tracker. Since the capsule was moving in a straight line, we can assume that the variation in position corresponds to the spring elongation. Therefore, the slope of the solid blue line provides an estimation of the spring constant. Such an estimation is 203.1 N/m, thus showing a 5.45% deviation from the nominal value.

3.3. In Vivo Validation

The feasibility of measuring resistant forces in the large intestine with the proposed wireless platform was then assessed *in vivo* on an anesthetized porcine model. The primary measure of interest was to acquire the static resistant force that a magnetically-driven capsule must overcome to begin its motion in a living colon. The dynamic behavior of the resistant force was also recorded, together with the position profile, as the capsule was moving toward the EPM under the effect of magnetic attraction.

Secondary measures of interest were the time to complete a single measurement, platform usability, assessment of the workspace, and robustness of the measurement with respect to electromagnetic interference. Reliability of the wireless link was also assessed.

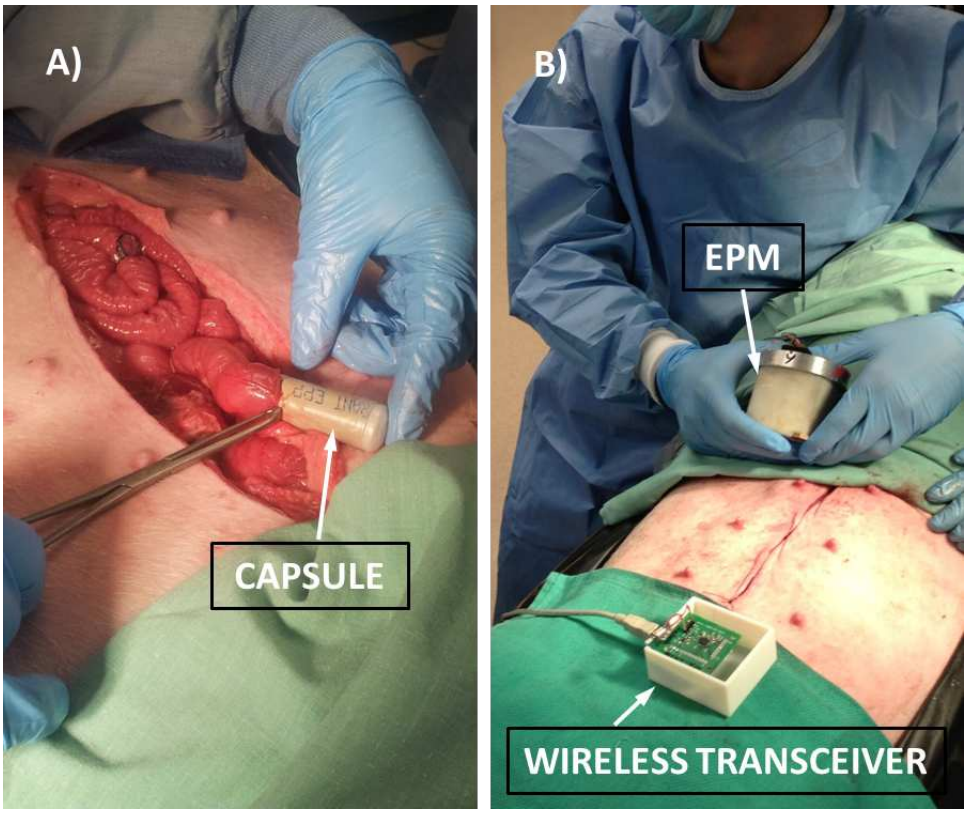

Figure 9. Photograph of the operative setup during the *in vivo* trial. (A) The wireless capsule being introduced in the porcine large intestine. (B) The surgical field during measurement.

The porcine surgery was performed at Vanderbilt University under IACUC protocol M/13/003. A 41-kg female Yorkshire swine was used for this study. After intravenous sedation, a laparotomy was performed to access the abdominal cavity. Then, the wireless capsule was inserted into a segment of the colon by intestinal ostomy, as represented in Fig. 9.A. The colon segment was straightened and sutured to the abdominal wall along the sagittal plane (two sutures spaces approximately 180 degree apart along the same circular segment) to prevent the capsule from dragging the tissue as it moved. The other

end of the segment was left unconstrained, so that the capsule was subjected to both circular and longitudinal muscle contraction. The length of the straightened segment was approximately 15 cm, thus allowing the capsule enough room to travel forward. A surgical marker was used to label 15 cm distal from the point of the suture. The midline incision was then sutured and the external transceiver was positioned on the porcine abdomen. As shown in Fig. 9.B, the EPM was placed parallel to the sagittal plane of the animal body, so that it would lie on the same vertical plane as the capsule and the straightened segment of large intestine. This satisfies the constraint defined in section 2.3.2 for a correct estimation of capsule motion profile. The acquisition software and the user interface were started, so that the user holding the EPM was able to see in real time both the intermagnetic force and the position and orientation of the capsule with respect to the EPM. The user interface also warned the user if the EPM and the capsule were both within the measurement workspace. Then, the operator moved the EPM closer to the capsule in steps of approximately 5 mm, until the user interface signaled that the capsule was starting to move. This process was repeated for ten times on the same segment of large intestine, always forcing the capsule to travel away from the anus. At the end of each measurement, the midline incision was opened and the capsule was moved backward to its starting position. For each trial, the platform recorded the intermagnetic force $\mathbf{F}_a$, the EPM-capsule separation distance $\mathbf{d}$, the capsule acceleration $\ddot{\mathbf{d}}$, and the time t_0 when the motion started as indicated by Eq. 10. From these data, the algorithm calculated the resistant force $\mathbf{F}_r$ and the capsule velocity $\dot{\mathbf{d}}$. During data analysis, the capsule velocity was used to confirm that the capsule was moving.

Two of the ten trials were excluded as the capsule did not accelerate fast enough to satisfy the trigger condition. The mean static resistant force $\mathbf{F}_r(t_0)$ recorded from the remaining eight trials was 0.21 N with a standard deviation of 0.06 N. The order of magnitude of this result agrees with previous literature data (Wang & Yan 2009, Zhang et al. 2012).

A plot of the modules of $\mathbf{F}_r$ and $\mathbf{d}$ for one trial is shown in Fig. 10. The adjustment in position of the EPM before the capsule started moving can be identified at the beginning of the two curves (dashed vertical line), where the position profile suddenly decreases and the force increases. The increase in the estimated $\mathbf{F}_r$ as the capsule moves towards the EPM can be explained by the exponential increase in the magnetic force, combined with the capsule decelerating at the end of the colon segment, where the tissue in between the capsule and the EPM prevents any further motion. The profiles reported in Fig. 10 suggest that the capsule was already moving before the platform detected its motion. However, before t_0, the acceleration was not strong enough to satisfy the condition in Eq. 10. As suggested in section 2.3.2, position $\mathbf{d}$ and velocity $\dot{\mathbf{d}}$ profiles can be analyzed to have a more sensitive condition for detecting the instant when capsule motion starts.

The time to complete a single measurement was 5 ± 1 minutes, from the moment that the EPM was introduced into the workspace to the instant when the capsule was placed back in the starting position. Thanks to the information available to the operator

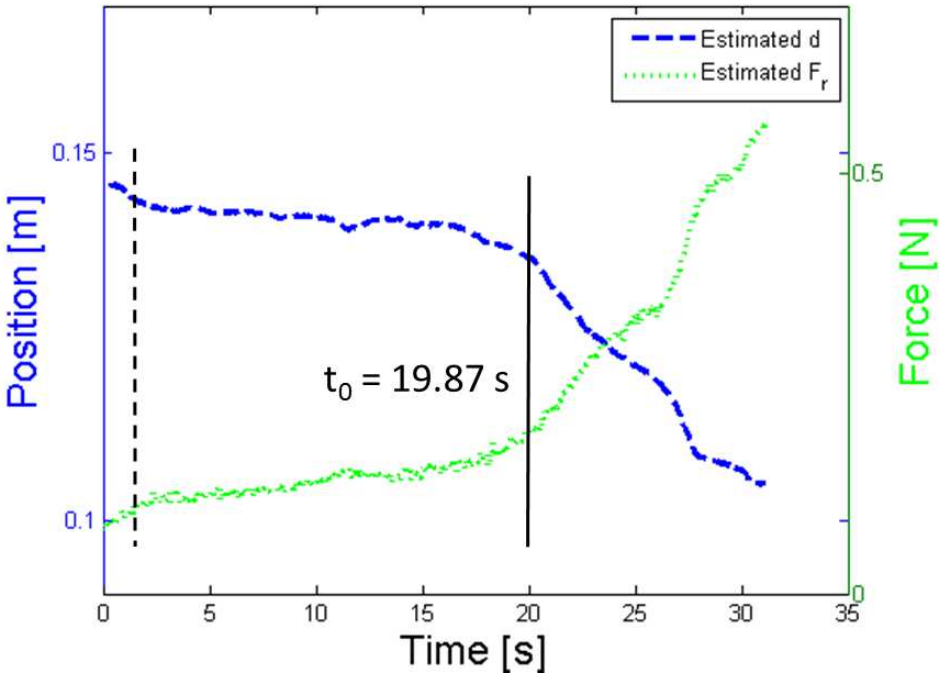

Figure 10. Plot of the modules of $\mathbf{F}_r$ and $\mathbf{d}$ acquired during the *in vivo* trial. The dashed vertical line indicates the instant when the EPM was moved closer to the capsule, while the solid vertical line indicates the instant when capsule motion started.

in real time, the platform was easy to use in all trials, and the protocol was performed without any need for adjustment. The workspace was confirmed to extend 15 cm away from each side of the EPM, and the effect of electromagnetic interference due to the equipment present in the operating room was negligible. The wireless link was reliable for about the 98% of data transmissions and battery operation was effective for the entire procedure. The *in vivo* experiment was one hour and fifteen minutes long.

4. Conclusions and Future Work

This manuscript introduces for the first time a wireless real-time platform for the *in vivo* measurement of the resistant force that a magnetically-driven capsule must overcome to move inside the GI tract. The platform takes advantage of a wireless capsule, magnetically coupled with an EPM, and is able to provide the real-time profile of both the intermagnetic force and capsule acceleration. The EPM-capsule separation vector and the capsule velocity are also estimated in real time, as well as the instant when the capsule starts moving under the effect of the external magnetic field. This information is used to derive the dynamic profile of the resistant force opposing magnetic attraction.

The platform was assessed via three-tier validation. First, the intermagnetic force and capsule position estimation was assessed with a dedicated benchtop trial using a robotic manipulator as a benchmark for position and a commercial load cell as reference

for the intermagnetic force. The average error in estimating the force and the position was less than 0.1 N and 10 mm, respectively. A second benchtop experiment was then performed to validate the dynamic reconstruction of $\mathbf{F}_r$ from the intermagnetic force and capsule motion estimation, using in this case a spring as reference for $\mathbf{F}_r$. The platform was able to estimate the spring constant with a relative error of 5.45%. Finally, the platform was assessed *in vivo* in a porcine colon model, where $\mathbf{F}_r$ was successfully measured.

While a statistically relevant study of the resistant forces of the porcine intestine was outside the scope of this study, this platform can be applied to more extensive biomechanical studies in the future (i.e., different segments of the GI tract can be investigated, and the force required to move with or against peristalsis can be measured). This would provide a quantitative understanding of resistant properties of the GI tract, paving the way for improved realistic biomechanical models.

Future improvements to the platform will aim to reduce the capsule size, extend the localization workspace, improve the localization accuracy, and add the sixth degree of freedom (i.e., rotation of the capsule about the $\mathbf{z}$ axis of the Global Cartesian coordinate system) to the localization algorithm. A promising approach of this direction consists in adopting the methods described in (Irimia & Bradshaw 2003, Irimia & Bradshaw 2004, Irimia & Bradshaw 2005) for forward modeling and inverse localization of electric currents and magnetic fields in the GI tract.

Real-time knowledge of both the intermagnetic force and capsule motion profile can be used for robotic-guided capsule endoscopy. To the best of our knowledge, none of the platforms proposed thus far for magnetic control of endoscopic capsules (Rey et al. 2012, Salerno et al. 2013, Di Natali et al. 2013, Yim & Sitti 2012, Mahoney & Abbott 2011, Zhou et al. 2013, Ciuti et al. 2010) implements a real-time tracking of capsule position and intermagnetic force. Integrating the methods proposed in this work in a platform such as the one reported in (Valdastri, Ciuti, Verbeni, Menciassi, Dario, Arezzo & Morino 2012) would enable "closed-loop control" of magnetic locomotion, by adjusting in real time the external source of the magnetic field to optimize the coupling with the capsule at any given point in time. Insufflation techniques such as the one proposed by the authors in (Valdastri, Ciuti, Verbeni, Menciassi, Dario, Arezzo & Morino 2012, Gorlewicz et al. 2013) would then prevent the magnetic capsule from becoming stuck along the way during the endoscopic examination.

Acknowledgment

This work was supported by the National Science Foundation under Grant No. CNS-1239355 and by the Broad Medical Research Program of The Broad Foundation. The authors would like to kindly acknowledge Mr. Phil Williams, Director of the Division of Surgical Research at Vanderbilt University Medical Center (VUMC), and all of the staff at the VUMC S.R. Light Surgical Facilities for Animal Trials for their precious time and assistance during the *in vivo* experiment.

References

Beccani M, Di Natali C, Sliker L, Schoen J, Rentschler M E & Valdastri P 2013 *IEEE Trans. Biomed. Eng* . in press, available on-line.

Bellini C, Glass P, Sitti M & Di Martino E S 2011 *Journal of the Mechanical Behavior of Biomedical Materials* **4**(8), 1727–1740.

Centers for Disease Control and Prevention 2013. URL http://www.cdc.gov.

Ciuti G, Salerno M, Lucarini G, Valdastri P, Arezzo A, Menciassi A, Morino M & Dario P 2012 *IEEE Trans. Robot.* **28**(2), 534–538.

Ciuti G, Valdastri P, Menciassi A & Dario P 2010 *Robotica* **28**(2), 199–207.

Di Natali C, Beccani M & Valdastri P 2013 *IEEE Trans. Magn.* **49**(7), 3524–3527.

Eliakim R, Yassin K, Niv Y, Metzger Y, Lachter J, Gal E, Sapoznikov B, Konikoff F, Leichtmann G, Fireman Z et al. 2009 *Endoscopy* **41**(12), 1026–1031.

Furlani E P 2001 Academic Press pp. 131–135.

Globocan 2008. URL http://globocan.iarc.fr/factsheets/cancers/colorectal.asp.

Gorlewicz J L, Battaglia S, Smith B F, Ciuti G, Gerding J, Menciassi A, Obstein K L, Valdastri P & Webster III R J 2013 *IEEE Transactions on Biomedical Engineering* **60**(5), 1225–1233.

Hounnou G, Destrieux C, Desme J, Bertrand P & Velut S 2002 *Surgical and Radiologic Anatomy* **24**(5), 290–294.

Irimia A & Bradshaw L A 2003 *Physical Review E* **68**(5), 051905.

Irimia A & Bradshaw L A 2004 *Physical Review E* **69**(5), 051920.

Irimia A & Bradshaw L A 2005 *Physics in medicine and biology* **50**(18), 4429.

Keller J, Fibbe C, Volke F, Gerber J, Mosse A C, Reimann-Zawadzki M, Rabinovitz E, Layer P, Schmitt D, Andresen V, Rosien U & Swain P 2011 *Gastrointestinal Endoscopy* **73**(1), 22–28.

Kim J S, Sung I H, Kim Y T, Kwon E Y, Kim D E & Jang Y 2006 *Tribology Letters* **22**(2), 143–149.

Kim J, Sung I, Kim Y, Kim D & Jang Y 2007 *Proceedings of the Institution of Mechanical Engineers, Part H: Journal of Engineering in Medicine* **221**(8), 837–845.

Kline S J & McClintock F A 1953 *Mechanical Engineering* **75**(1), 3–8.

Lyle A B, Luftig J T & Rentschler M E 2013 *Tribology International* **62**, 171–176.

Mahoney A W & Abbott J J 2011 *Applied Physics Letters* **99**(13), 134103–134103.

Mahoney A W & Abbott J J 2012 *in* 'IEEE International Conference on Biomedical Robotics and Biomechatronics (BioRob)' pp. 1632–1637.

Miller E & Ullrey D 1987 *Annual review of nutrition* **7**(1), 361–382.

Miller K M, Mahoney A W, Schmid T & Abbott J J 2012 *in* 'IEEE/RSJ International Conference on Intelligent Robots and Systems (IROS)' pp. 1994–1999.

Petruska A & Abbott J 2013 *IEEE Trans. Magn.* **49**(2), 811–819.

Pox C, Schmiegel W & Classen M 2007 *Endoscopy* **39**(02), 168–173.

Rey J F, Ogata H, Hosoe N, Ohtsuka K, Ogata N, Ikeda K, Aihara H, Pangtay I, Hibi T, Kudo S & Tajiri H 2012 *Gastrointestinal Endoscopy* **75**(2), 373–381.

Salerno M, Rizzo R, Sinibaldi E & Menciassi A 2013 *in* 'IEEE International Conference on Robotics and Automation (ICRA)' pp. 5334–5339.

Samsom M, Smout A, Hebbard G, Fraser R, Omari T, Horowitz M & Dent J 1998 *Neurogastroenterology and Motility* **10**(2), 139–148.

Simi M, Valdastri P, Quaglia C, Menciassi A & Dario P 2010 *IEEE/ASME Trans. Mechatronics* **15**(2), 170–180.

Sliker L J, Kern M D, Schoen J A & Rentschler M E 2012 *Surgical Endoscopy* **26**(10), 2862–2869.

Spada C, De Vincentis F, Cesaro P, Hassan C, Riccioni M E, Grazioli L M, Bolivar S, Zurita A & Costamagna G 2012 *Therapeutic Advances in Gastroenterology* **5**(3), 173–178.

Terry B S, Passernig A C, Hill M L, Schoen J A & Rentschler M E 2012 *Journal of the Mechanical Behavior of Biomedical Materials* **15**, 24–32.

Toennies J L, Tortora G, Simi M, Valdastri P & Webster III R J 2010 *Proceedings of the Institution of*

Mechanical Engineers, Part C: Journal of Mechanical Engineering Science **224**(7), 1397–1414.

Valdastri P, Ciuti G, Verbeni A, Menciassi A, Dario P, Arezzo A & Morino M 2012 *Surgical Endoscopy* **26**(5), 1238–1246.

Valdastri P, Simi M & Webster III R J 2012 *Annual Review of Biomedical Engineering* **14**, 397–429.

Valdastri P, Webster III R J, Quaglia C, Quirini M, Menciassi A & Dario P 2009 *IEEE Trans. Robot.* **25**(5), 1047–1057.

Wang K D & Yan G Z 2009 *Measurement Science and Technology* **20**(1), 015803.

Wang X & Meng M Q 2010 *Proceedings of the Institution of Mechanical Engineers, Part H: Journal of Engineering in Medicine* **224**(1), 107–118.

Yim S & Sitti M 2012 *IEEE Trans. Robot.* **28**(1), 183–194.

Zhang C, Liu H, Tan R & Li H 2012 *Tribology Letters* **47**(2), 295–301.

Zhou H, Alici G, Than T D & Li W 2013 *IEEE/ASME Trans. Mechatronics* **18**(5), 1555–1562.